

Investigation of a Shock-Detecting Sensor for Filtering of High-Order Compact Finite Difference Schemes

M. Khoshab¹, A. A. Dehghan¹, H. Mahmoodi Darian², and *V. Esfahanian³

¹Faculty of Mechanical Engineering, Yazd University, Yazd, Iran

²Department of Basic Engineering Science, College of Engineering, University of Tehran, Tehran, Iran

³Vehicle, Fuel, and Environment Research Institute, University of Tehran, Tehran, Iran

*Corresponding author: evahid@ut.ac.ir

Abstract

High-order simulation of flows containing shock waves is an extremely difficult task due to the discontinuous changes in flow properties across the shock. The present work investigates a shock-detecting sensor for filtering of high-order compact finite-difference schemes to examine the shock-capturing in direct simulation of Navier-Stokes solver. Based on the accuracy and minimum dissipation error, the shock-detecting sensor is selected for the DNS studies. The implementation of high resolution simulations using sixth-order compact schemes with a fourth-order two-register Runge-Kutta method is validated through selective test problems. Through several numerical experiments (including an inviscid shock/vortex interaction, a viscous shock/vortex interaction, and a shock/mixing layer interaction) the accuracy of the nonlinear filter is examined. The results indicate that the shock-detecting sensor works well, and can be used for future simulations of turbulent flows containing shocks.

Keywords: shock-detecting sensor, shock-capturing, nonlinear filter, high-order scheme.

Introduction

Numerical investigation of high speed turbulent flows, including vortices and shocks, can be found in many engineering applications. In order to resolve a wide range of length and time scales in these flows, the compact methods proposed by Lele (1992) are typically used in DNSs of turbulent flows as well as in computational aeroacoustics (CAA). The compact schemes contain a smaller truncation error compared with non-compact schemes of the same order, and required smaller numerical stencil size.

As mention above, the accurate compact central scheme is required to preserve the vortical flow structures; however, it does not have shock capturing capability (Lo, Blaisdell, & Lyrintzis, 2010). Meanwhile, the traditional second-order accurate shock capturing schemes are usually not suitable for turbulence simulations due to dissipative feature. Therefore, high-order TVD schemes, the extension of Godunov algorithm using high-order reconstructions (Colella & Woodward, 1984; Van Leer, 1974) and the creation of essentially non-oscillatory (ENO) (Harten & Osher, 1985; Harten, Engquist, Osher, & Chakravarthy, 1987; Harten, Osher, Engquist, & Chakravarthy, 1986; Shu & Osher, 1988, 1989) and weighted essentially non-oscillatory (WENO) (Jiang & Shu, 1996; Liu, Osher, & Chan, 1994) schemes are developed to enhance the methods to have shock capturing ability. Assessment of the

WENO scheme for numerical simulations of compressible turbulence with shock waves shows that the WENO scheme can serve as a reliable tool for DNS of compressible turbulence (Chaudhuri, Hadjadj, Chinnayya, & Palerm, 2010; Johnsen et al., 2010).

The complicated algorithms of the above methods and some deficiencies encourage a few researchers to use high-order compact finite-difference schemes with a special kind of shock detecting sensor (Bogey, de Cacqueray, & Bailly, 2009; Hadjadj, Yee, & Sjögren, 2012; Mahmoodi Darian, Esfahanian, & Hejranfar, 2011; Sjögren & Yee, 2004; Visbal & Gaitonde, 2005; Yee, Sandham, & Djomehri, 1999; Yee & Sjögren, 2008). In other words, a shock-detecting sensor restricts the use of second-order filter to regions near shocks, therefore, the dissipation can be applied only in the large gradient regions (i.e. shocks) and the spatial higher-order filter is applied to other smooth regions instead. In addition, since these hybrid filters can be applied once to the solutions after each full time step, the computational cost is considerably less than that of traditional shock capturing schemes.

The motivation of the present work is to develop a reliable numerical solver in a fully compressible formulation using high-order accurate schemes and extending the shock-detecting sensor introduced by (Mahmoodi Darian et al., 2011) to the general curvilinear coordinates for simulation of subsonic turbulence, based on direct numerical simulation (DNS), and supersonic flows with vortical flows interacting with shocks waves.

Numerical Methods

Governing Equation and Discretization Scheme

Governing equations are the unsteady dimensionless compressible Navier-Stokes equations in curvilinear coordinates (ξ, η, ζ) , are written in conservative form. The use of low-dissipation, high-order schemes is an essential ingredient when computing compressible flows. The objective is to avoid excessive numerical dissipating of the flow features over a wide range of length scales. For instance, the family of compact schemes can be a good choice to achieve this goal. The computation of all derivatives is carried out by a sixth-order compact central scheme (Lele, 1992). On near-boundary nodes, accurate non-central or one-sided compact schemes are considered. In this study, the time integration is performed by means of a fourth-order accurate Runge-Kutta method with two-register storage (Kennedy, Carpenter, & Lewis, 2000). In addition, non-reflecting boundary conditions for compressible flow in curvilinear coordinates (Chen & Zha, 2006) are used.

Description of the sensor and the nonlinear filter

As the filter form introduced in (Mahmoodi Darian et al., 2011), the numerical filter equation in the conservative form is

$$\tilde{U}_j^{n+1} = U_j^{n+1} + \frac{\Delta t}{\Delta \xi} (\tilde{F}_{j+1/2} - \tilde{F}_{j-1/2}) \quad (1)$$

where Δt is the time-step and $\Delta \xi$ is the grid size in ξ direction. The $\Delta \xi$ and $\Delta \eta$ is equal to 1. For a $2m$ th-order explicit linear filter one can have:

$$\tilde{F}_{j+1/2}^{(m)} = (-1)^{m-1} \epsilon^{(m)} \tilde{\lambda}_\xi (\Delta \nabla)^{m-1} \Delta U_j \quad (2)$$

where $\tilde{\lambda}_\xi$ is the modified characteristic velocity, in curvilinear coordinates, $\epsilon^{(m)}$ is the dissipation coefficient and Δ and ∇ are the forward and backward difference operators, which are defined by

$$\Delta U_j = U_{j+1} - U_j, \quad \nabla U_j = U_j - U_{j-1}$$

The modified characteristic velocity, $\tilde{\lambda}_\xi$ is a weighted average between maximum characteristic velocity in the entire computational field, $\lambda_{\max, global}$, and local characteristic velocity, $\lambda_{j+1/2}$:

$$\lambda_\xi = \omega_\lambda \lambda_{\max, global} + (1 - \omega_\lambda) \lambda_{j+1/2}$$

where λ_j is the characteristic velocity (an eigenvalue of the flux jacobian).

There are good reasons that the second-order linear filter is suitable for discontinuous regions which is not the case for the higher-order linear filters. On the other hand, the high-order linear filters have desirable properties in smooth regions. Consequently, it is desirable to have a nonlinear filter which acts as a second-order linear filter near the discontinuities and behaves as a high-order linear filter in smooth regions (Bogey et al., 2009; Visbal & Gaitonde, 2005). In this regard, we write the numerical filter flux as a combination of the second- and a higher-order filter flux:

$$\tilde{F} = \omega_1 \tilde{F}^{(1)} + \omega_m \tilde{F}^{(m)}, \quad m > 1 \quad (3)$$

where ω_1 and ω_m are the nonlinear weights controlling the amount of the second- and $2m$ th-order filters. The proper design of these weights is essential to have high accuracy in smooth regions and to obtain non-oscillatory sharp discontinuities. The following weights are proposed by (Mahmoodi Darian et al., 2011):

$$\omega_1 = 1 - \exp(-c_e e_{j+1/2}^2), \quad \omega_m = \exp(-c_e e_{j+1/2}^2) \quad (4)$$

where c_e is a positive constant number. This definition ensures both ω_1 and ω_m are between 0 and 1. Note that $c_e = 0$ reduces the filter to the $2m$ th-order linear filter and $c_e \rightarrow \infty$ corresponds to the second-order linear filter. The term $e_{j+1/2}$ is a kind of smoothness measurement which is defined as

$$e_{j+1/2} = \max(e_j, e_{j+1}), \quad e_j = \frac{|\hat{U}_j - U_j|}{D_j} \quad (5)$$

and \hat{U}_j is the interpolated value of U at the point x_j using the neighboring points $\{U_{j\pm k}\}_{k=1, \dots, m'}$, which is computed as

$$\hat{U}_j = U_j - \frac{(-1)^{m'}}{\binom{2m'}{m'}} (\Delta \nabla)^{m'} U_j, \quad \binom{2m'}{m'} = \frac{(2m')!}{(m')!(m')!} \quad (6)$$

Therefore, the numerator in (5) is the error of a $2m'$ th-order interpolation. The denominator D_j is a scaling value. For more details see the (Mahmoodi Darian et al., 2011).

In equation (5) some sort of scaling is needed to have a measure to distinguish the large interpolations errors from the small ones. For this reason, we propose the following scaling

$$D_j = c_s S_g + (1 - c_s) S_l, \quad S_g = U_{\max}^g - U_{\min}^g, \quad S_l = U_{\max}^l - U_{\min}^l \quad (7)$$

where S_g and S_l are the global and local scales, respectively. Also, c_s is the scaling constant which is a positive number smaller than unity. The global and local maximum and minimum are defined as:

$$\begin{aligned} U_{\max}^g &= \max_k(U_k), & U_{\min}^g &= \min_k(U_k), & 1 \leq k \leq j_{\max} \\ U_{\max}^l &= \max_k(U_k), & U_{\min}^l &= \min_k(U_k), & j-m' \leq k \leq j+m' \end{aligned} \quad (8)$$

Numerical Experiments

1D problems: Linear wave equation and Shock-tube

In the first test case, the linear wave equation is solved. The initial condition is a periodic function similar to work of Mahmoodi Darian et al., (2011). The equation is solved with a uniform grid of $\Delta x = 1/200$ and a fixed time-step of $\Delta t = 0.002$ up to $t = 6$ corresponding to three time periods. Both linear and nonlinear filters produce nearly the same results in the smooth regions as shown in Fig. 1.

In the second test case, a well-known Riemann problem introduced by Sod (1978) is solved. The equations are the compressible one-dimensional Euler equations. The numerical solutions are obtained at $t = 2$ with a uniform grid of 400 points and CFL=0.2. In Fig. 2 the results are compared with analytical solution.

In both test cases, it can be seen that the non linear filter capture discontinuities sharply.

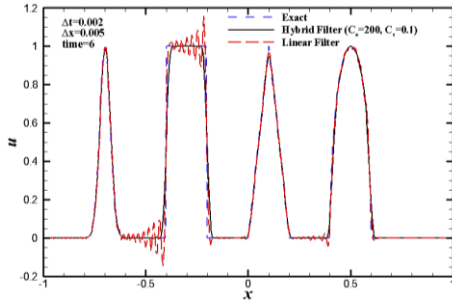


Figure 1. Linear wave equation

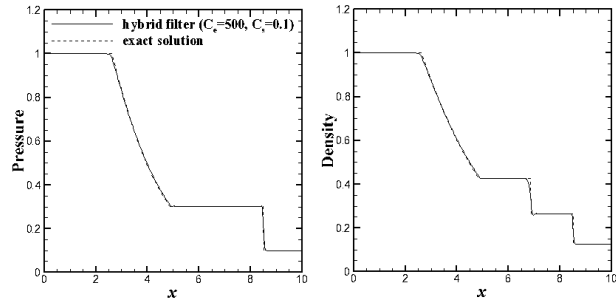


Figure 2. Pressure and density distribution

2D Inviscid Shock-Vortex interactions

This is a two-dimensional test case that describes the interaction between a stationary shock and a vortex (Jiang & Shu, 1996). A stationary Mach 1.1 shock is positioned at $x = 0.5$ and normal to the x -axis similar to work of (Jiang & Shu, 1996).

The results are obtained with a uniform grid of 251×101 and CFL=0.1. The coefficients c_e , c_s and ω_λ for the nonlinear filter are set to 200, 0.1 and 1, respectively. The non-reflecting far-field boundary conditions are applied in the top and bottom faces and the non-reflecting outflow boundary condition is set at the downstream. The pressure contours are displayed in Fig. 3. Eighteen contour lines from 0.59 to 0.78 are used. It can be seen that the sensor resolve the vortex properly. Fig. 4(a) displays the pressure distribution along the $y = 0.5$ section at $t = 0.6\sqrt{\gamma}M_\infty$ before and after the shock. The pressure distributions in some extreme zones are zoomed in figures 4(b)-4(d).

The effect of grid on the sensor resolution is presented in Fig. 5(a) by the pressure distribution along the $y=0.5$ section. It can be seen that the shock is captured by nonlinear filter even in the coarse grid. The pressure distributions in some extreme zones are zoomed in figures 5(b)-5(d). The nonlinear sensor is designed for wide range of shock strength. In the Fig. 6(a), it can be seen that the strong shock is captured by nonlinear sensor properly. The pressure distributions in some extreme zones are zoomed in figures 6(b)-6(d). In the present case, the slip-wall (reflecting) boundary conditions are applied in the top and bottom faces due to investigation on the effects of shock reflection on the results.

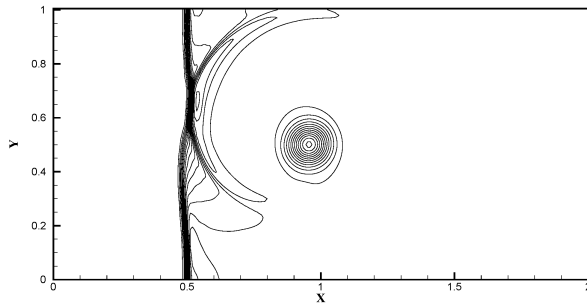


Figure 3. Pressure contours for the 2D shock–vortex interaction at $t = 0.6\sqrt{\gamma}M_\infty$ (18 contours from 0.59 to 0.78).

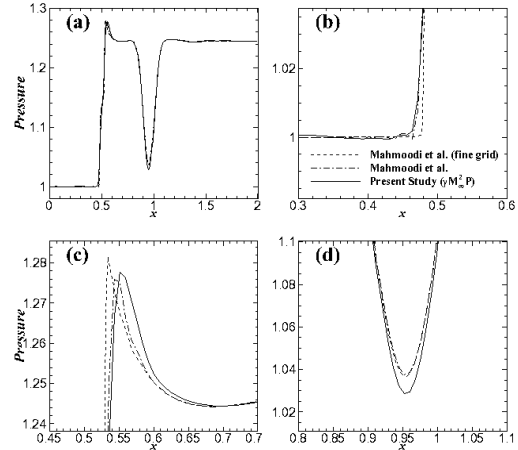


Figure 4. Pressure distribution along the $y = 0.5$ section at $t = 0.6\sqrt{\gamma}M_\infty$ for the Inviscid shock–vortex interaction.

2D Viscous Shock-Vortex interactions

This case is the two-dimensional compressible vortex convected through a normal shock. This is a typical test used to evaluate the diffusive or dispersive property of scheme i.e. used to evaluate of shock-capturing scheme. The configuration corresponds to an isolated Taylor vortex with a Mach number $M_\infty = 1.1588$ and a Reynolds number $Re = 2000$, is initially superimposed on a uniform flow field aligned along the x -direction similar to (Lo et al., 2010). The CFL number is set to 0.1 with $c_e = 200$, $c_s = 0.1$ and $\omega_\lambda = 1$ for the nonlinear filter. The non-reflecting far-field boundary conditions are applied in the top and bottom faces and the non-reflecting outflow boundary condition is used at the downstream.

The pressure contour at $t = 0.7$ is shown in Fig. 7. Figure 8 shows the density distributions at $t = 0.7$ along side of the results of (Lo et al., 2010). It can be seen that the sensor resolve the vortex properly in the viscous field. Along the line of $y = 1$, the vortex core at $t = 0.7$ is located at $x = 1.16$ and a downstream propagating acoustic wave is around $x = 1.8$.

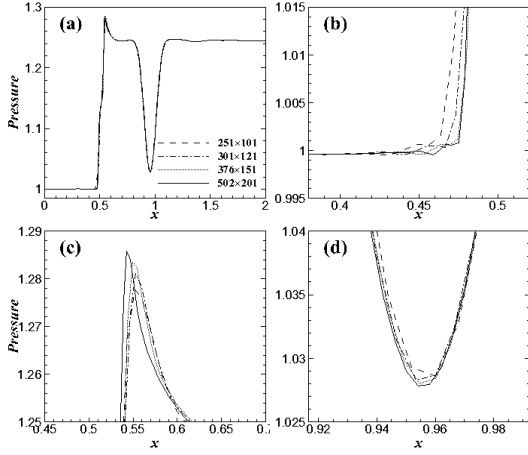


Figure 5. Effect of grid on the pressure distribution along the $y = 0.5$ section at $t = 0.6\sqrt{\gamma}M_\infty$.

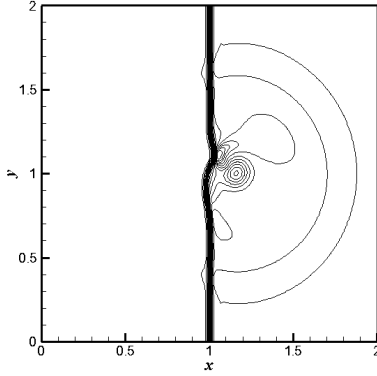


Figure 7. Pressure contours at $t=0.7$ by a grid 203×203 (20 contours from 0.527 to 0.817).

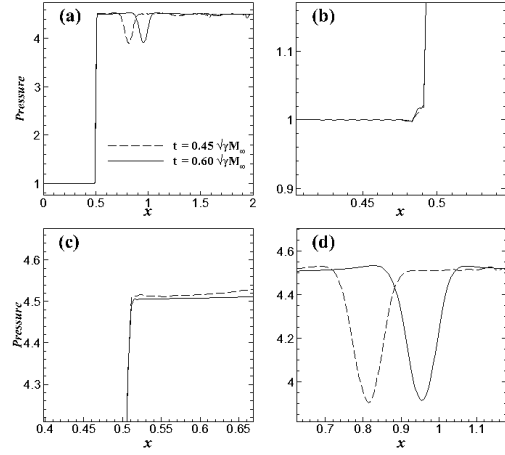


Figure 6. Pressure distribution along the $y = 0.5$ section for strong shock $M_\infty = 2.0$ (grid 502×201).

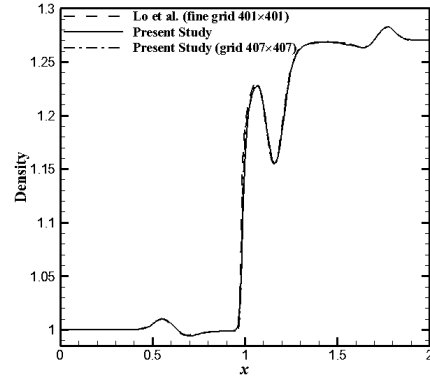


Figure 8. Instantaneous density distribution at $t=0.7$ along $y=1$ by a grid 203×203 and 407×407 .

Shock-Mixing layer interactions

This case is used to evaluate the performance of the shock capturing schemes for interactions of shock waves and shear layers (Lo et al., 2010; Yee et al., 1999). Figure 9 shows the schematic view of the flow configuration. An oblique shock originating from the upper-left corner interacts with shear layers where the vortices arising from shear layer instability. This oblique shock is deflected by the shear layer and then reflects from the bottom slip wall. Simultaneously, an expansion fan forms above the shear layer and at the downstream, a series of shock waves form around the vortices. The outflow boundary has been arranged to be supersonic everywhere. The computational domain were taken to be $L_x = 200$ and $L_y = 40$. The inflow boundary condition is specified with a hyperbolic tangent profile (see the stream (1) and (2) in Fig. 9),

$$u = 2.5 + 0.5 \tanh(2\hat{y}), \quad \text{with } \hat{y} = y - L_y / 2$$

The only transverse-velocity fluctuations are added to the inflow as:

$$v' = \sum_{k=1}^2 a_k \cos(2\pi kt / T) + \phi_k \exp(-\hat{y}^2 / b)$$

with the period $T = \lambda / u_c$, convective velocity $u_c = 2.68$, the wavelength $\lambda = 30$ and the other constants are given by $b = 10$, $a_1 = a_2 = 0.05$, $\phi_1 = 0$ and $\phi_2 = \pi / 2$, similar to (Yee et al., 1999). The two streams have the same inflow pressure and stagnation enthalpies. All properties are normalized by the properties of the stream (1).

For the left and top boundaries, supersonic inflow imposed, whereas slip-wall conditions are assumed at the bottom boundary to avoid any boundary-layer formation and subsequent complexities arising from the shock/boundary layer interaction. At the outflow the non-reflecting outflow conditions are assumed. A grid dependency study using four different meshes, namely mesh-1 512×128 (uniform and non-uniform): mesh-2: 1024×256 , mesh-3: 2048×512 and mesh-4: 4096×1024 (about 4.2 million points). Figures 10 show the Numerical schlieren based on density, pressure and shadowgraph contours. From the figures, it can be seen that the shapes of the vortices are resolved properly, and the shocklets generated by the vortices in the downstream region. The shock-detecting sensor provides high quality vortices and downstream shocklet resolution.

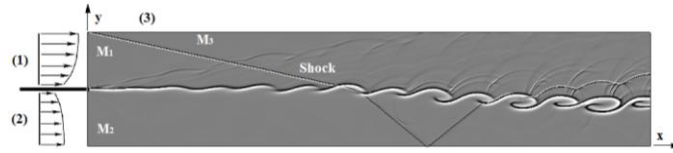


Figure 9. Schematic view of the shock/mixing-layer interaction configuration

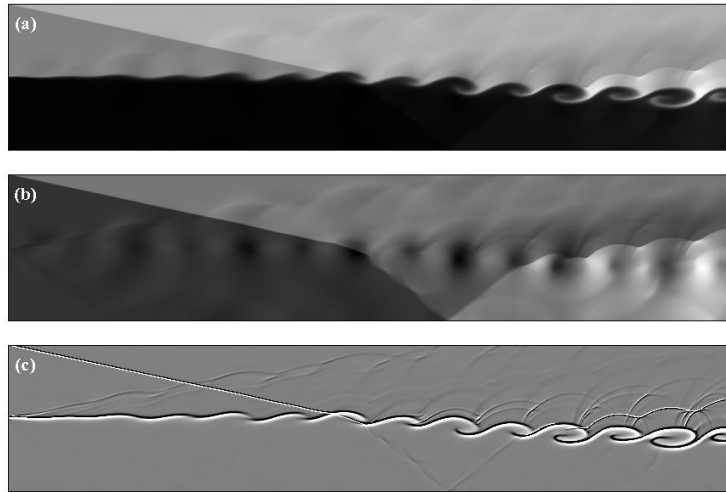


Figure 10. Numerical schlieren based on (a) density, (b) pressure, and (c) shadowgraph, for a 2048×512 grid with $c_e = 200$, $c_s = 0.1$ and $\omega_\lambda = 1$ for the filter.

Conclusions

In the present study, a Navier-Stokes computational methodology for turbulent supersonic flows based on high-order compact finite-difference schemes is developed and the shock-detecting sensor has been extended and tested for several test cases. The sensor is based on an interpolation error scaled by a suitable scaling value which scales the large errors by their local scale and the small errors by a proportion of the global scale. The sensor is developed in curvilinear coordinates and tested through several test cases including a 2D stationary shock with a moving vortex, and a 2D shock/mixing layer interaction. The results indicate that the shock-detecting sensor works well, and can be used for future simulations of turbulent flows containing shocks.

References

- Bogey, C., de Cacqueray, N., & Bailly, C. (2009). A shock-capturing methodology based on adaptive spatial filtering for high-order non-linear computations. *Journal of Computational Physics*, 228(5), 1447–1465.
- Chaudhuri, A., Hadjadj, A., Chinnayya, A., & Palerm, S. (2010). Numerical Study of Compressible Mixing Layers Using High-Order WENO Schemes. *Journal of Scientific Computing*, 47(2), 170–197.
- Chen, X., & Zha, G.-C. (2006). Implicit application of non-reflective boundary conditions for Navier–Stokes equations in generalized coordinates. *International Journal for Numerical Methods in Fluids*, 50(7), 767–793.
- Colella, P., & Woodward, P. R. (1984). The piecewise parabolic method (PPM) for gas-dynamical simulations. *Journal of computational physics*, 54(1), 174–201.
- Hadjadj, A., Yee, H. C., & Sjögren, B. (2012). LES of temporally evolving mixing layers by an eighth-order filter scheme. *International Journal for Numerical Methods in Fluids*, 70, 1405–1427.
- Harten, A., & Osher, S. (1985). Uniformly high-order accurate non-oscillatory schemes, 1. *SIAM Journal on Numerical Analysis*, 24(2), 279–309.
- Harten, Ami, Engquist, B., Osher, S., & Chakravarthy, S. R. (1987). Uniformly high order accurate essentially non-oscillatory schemes. III. *Journal of Computational Physics*, 71(2), 231–303.
- Harten, Ami, Osher, S., Engquist, B., & Chakravarthy, S. R. (1986). Some results on uniformly high-order accurate essentially nonoscillatory schemes. *Applied Numerical Mathematics*, 2(3), 347–377.
- Jiang, G.-S., & Shu, C.-W. (1996). Efficient implementation of weighted ENO schemes. *Journal of Computational Physics*, 126(1), 202–228.
- Johnsen, E., Larsson, J., Bhagatwala, A. V., Cabot, W. H., Moin, P., Olson, B. J., ... Lele, S. K. (2010). Assessment of high-resolution methods for numerical simulations of compressible turbulence with shock waves. *Journal of Computational Physics*, 229(4), 1213–1237.
- Kennedy, C. A. C. A., Carpenter, M. H., & Lewis, R. M. (2000). Low-Storage, Explicit Runge-Kutta Schemes for the Compressible Navier-Stokes Equations. *Applied Numerical Mathematics*, 35(3), 177–219.
- Lele, S. K. (1992). Compact finite difference schemes with spectral-like resolution. *Journal of Computational Physics*, 103(1), 16–42.
- Liu, X. D., Osher, S., & Chan, T. (1994). Weighted Essentially Non-Oscillatory Schemes. *Journal of Computational Physics*, 115(1), 200–212.
- Lo, S., Blaisdell, G. A., & Lyrintzis, A. S. (2010). High-order shock capturing schemes for turbulence calculations. *International Journal for Numerical Methods in Fluids*, 62, 473–498.
- Mahmoodi Darian, H., Esfahanian, V., & Hejranfar, K. (2011). A shock-detecting sensor for filtering of high-order compact finite difference schemes. *Journal of Computational Physics*, 230(3), 494–514.
- Shu, C.-W., & Osher, S. (1988). Efficient implementation of essentially non-oscillatory shock-capturing schemes. *Journal of Computational Physics*, 77(2), 439–471.
- Shu, C.-W., & Osher, S. (1989). Efficient implementation of essentially non-oscillatory shock-capturing schemes. II. *Journal of Computational Physics*, 83(1), 32–78.
- Sjögren, B., & Yee, H. C. (2004). Multiresolution wavelet based adaptive numerical dissipation control for high order methods. *Journal of Scientific Computing*, 20(2), 211–255.
- Sod, G. (1978). A survey of several finite difference methods for systems of nonlinear hyperbolic conservation laws. *Journal of Computational Physics*, 27, 1–31.
- Van Leer, B. (1974). Towards the ultimate conservative difference scheme. II. Monotonicity and conservation combined in a second-order scheme. *Journal of Computational Physics*, 14(4), 361–370.
- Visbal, M. R., & Gaitonde, D. V. (2005). Shock capturing using compact-differencing-based methods. In *43rd AIAA Aerospace Sciences Meeting and Exhibit* (p. 2005).
- Yee, H. C., Sandham, N. D., & Djomehri, M. J. (1999). Low-Dissipative High-Order Shock-Capturing Methods Using Characteristic-Based Filters. *Journal of Computational Physics*, 150(1), 199–238.
- Yee, H. C., & Sjögren, B. (2008). Adaptive filtering and limiting in compact high order methods for multiscale gas dynamics and MHD systems. *Computers & Fluids*, 37(5), 593–619.